Repeatability of vessel density measurement in human skin by OCT-based microangiography

Shaojie Men, **Chieh-Li Chen**, **Wei Wei**, **Ting-Yu Lai**, **Shaozhen Song**, and **Ruikang K. Wang**[*]
Department of Bioengineering, University of Washington, Seattle, WA, USA

Abstract

Purpose—To investigate the repeatability of vessel density measurement at human arm skin in healthy subjects with OCT-based microangiography (OMAG).

Methods—Four locations including volar wrist, volar forearm, shoulder and volar upper arm were scanned using an optimized swept source OCT system, working at center wavelength of 1300 nm and A-line rate of 100 kHz. Three scans were acquired at each location at the same visit. Vascular images of papillary dermis, reticular dermis and the whole dermis layer were generated with OMAG processing and automatic segmentation algorithms. The vessel density (VD) of each layer was calculated based on vascular images, and the repeatability of the VD at the same physiological location was thereafter assessed.

Results—Fifteen healthy volunteers were included. High repeatability of VD was found for wrist, forearm, shoulder and upper arm (coefficient of variation (CV) = 2.4, 2.7, 2.7, 2.0, and intraclass correlation coefficient (ICC) = 0.906, 0.854, 0.943, 0.916, respectively). The VD measurements showed no significant difference between the four locations in any of the three layers, i.e. papillary layer ($P = 0.1063$), reticular layer ($P = 0.3371$) and whole dermis layer ($P = 0.3233$).

Conclusion—Quantification of VD by using OCT/OMAG is repeatable when imaging skin tissue beds in healthy individuals.

Keywords

optical coherence tomography angiography; optical microangiography; human skin; vessel density; repeatability

1. Introduction

In recent years, skin microcirculation has attracted much attention in clinical medicine due to its close association with numerous diseases, such as inflammation (1), malignancies (2), diabetes (3), hypertension and cardiovascular disease (4). It has been demonstrated that changes in structures and patterns of microcirculation can be considered as an early

Disclosure
The authors state no financial conflict of interest for this study.

symptom to distinguish pathema from normal conditions (5,6). Therefore, being able to qualitatively visualize and quantitatively measure skin microvasculature are critical in detecting the changes at the earliest possible time point and potentially identifying diseases prior to clinical diagnosis (7).

Currently, several optical-based imaging techniques have been employed to investigate the skin microcirculation system. Capillaroscopy is one of the most prevailing non-invasive method in the microvascular study (8). With a magnification up to 200x, it can visualize the capillaries and provide microcirculation pattern especially in nail fold, lips and mouth. Laser-Doppler perfusion imaging (LDPI) is another non-invasive technique that can be used to obtain the perfusion images and measure the average speed of flow by using the Doppler frequency shifts with scanning light scattered from moving blood cells (9). Photoacoustic microscopy (PAM) is an optical-ultrasonic dual-modality imaging technique capable of extracting vascular image map in vivo, which has been applied to study the microcirculation in nevus (10), nail fold (11) and palm (12).

Optical coherence tomography (OCT) is a promising imaging technique, allowing non-invasive, three-dimension, high resolution imaging of biological tissues (13,14). As a functional variation of OCT, optical microangiography (OMAG) is capable of extracting vascular system map from the structural tissue with the resolution up to capillary level (15–18). Nowadays, OMAG technique has been demonstrated as a powerful tool applying in dermatology to qualitatively visualize microvascular structures and make quantitative measurements on vessel density (19–23). However, no study has demonstrated the repeatability of vessel density in OCT images. Knowledge of the reliability of vessel density in OCT images is essential not only for the improvement in clinical practice, but also in the continuous development of OCT based angiography techniques for dermatology applications. In the present study, we aim to use OMAG to visualize the vascular imaging and quantify the vessel density of human arm skin in healthy subjects. We evaluate the repeatability of the measurement as well to inspect the reliability of our instrument as a diagnostic tool in clinical practice. To the best our knowledge, this is the first study that demonstrates the repeatability of quantification of vessel density in OCT angiography images of human skin.

2. Method

Subjects and System setup

This study was approved by the institutional review board of University of Washington. Written informed consents were obtained from all the volunteers before imaging, following the Declaration of Helsinki. For this prospective study, volunteers aged > 18 years old with no history of dermatology and medical issues on the interest regions were include. Exclusion criteria were any clinical or history evidence of skin disease, wound, nevus, birthmark or tattoo in the scanned regions.

Four locations on the right arm, including volar wrist, volar forearm, shoulder and volar upper arm, were scanned using a 100-kHz prototype swept source OCT (SS-OCT) system. The SS-OCT system worked at a center wavelength of 1300 nm and an effective axial

resolution of 15 μm, similar to our previous studies (24). A handheld probe specifically designed for dermatological applications was adopted for easy access to various skin sites. Before imaging, each subject seated and acclimatized to the imaging position for 5 min. The probe was held gently in contact with the skin of the subject, where a drop of mineral oil was added as the refractive index matching medium to reduce the specular reflection at surface. The OCT beam was focused at ~250 μm below the skin surface for subsurface imaging of the vascular network in the dermis layer. With a 5x microscope objective lens, the lateral resolution was measured to be 15 μm at the focus.

Imaging protocol

Imaging protocol was similar to that used for optical coherence tomography angiography (OCTA) data acquisition that was adopted in retinal imaging (16,18,25,26). In this protocol, 500 transverse positions with 5 repetitions at each Y-direction (slow scan) position (a total of 2500 cross-sectional B-frames) were acquired. Along the X-direction (fast scan), galvanometric scanner was operated at a frame rate of 167 Hz with 500 A-lines and 100 fly-back lines (duty cycle 83%). Such scanning covered a field of view (FOV) of 7×7 mm^2 with sampling spacing of 14 μm between adjacent A-lines and 14 μm between adjacent B-frames. The total acquisition time of each 3D volume (corresponding to 500 (X) $\times$ 2500 (Y) $\times$ 1280 (Z) voxels) was 15 s, which is tolerable for human subjects. Every subject went through three repeated imaging sessions in a single visit by the same operator. The imaging region of interest was re-positioned in the next scan, and the timing separation between scans was roughly 5 min.

The OCT cross-sectional structural image was obtained by averaging the 5-repeated OCT signals at the same spatial position. Therefore, one volume scan consisted of 500 such cross-sectional OCT images to reveal depth-resolved microstructural tissue information. To delineate the microvascular network, inter-B-frame complex ED-OMAG algorithm was applied (27,28) to the 5 repeated B-frames at each position, generating 500 cross-sectional blood flow images and further reconstructed into one 3D dataset. Vasculatures of the papillary dermis layer and the reticular dermis layer were separated through an automatic segmentation approach (29,30). By using the structural images, the boundary of the epidermis and dermis was determined by detecting the peak value of the OCT signal intensity. As shown in Figure 1(b) and (c), the first dashed line from the top is considered as the interface between the epidermis layer and dermis layer. Then the interface (the first line) was moved downward (depth direction) 150 μm and 850 μm, respectively, which were considered as the boundary (the second line) of the papillary layer and the reticular layer and the lower bound (the third line) of the dermis layer. The three boundaries were applied to the vascular image to finish the automatic segmentation. The vascular enface images for papillary layer, reticular layer, and the whole dermis layer were generated by maximum intensity projecting (MIP).

Vessel density

To calculate vessel density, firstly, all the *en face* images were binarized. The threshold of each image was determined by the mean pixel value. Values that are below the threshold were set to zero (black) and those above the threshold were set to one (white). The white

pixels represent the area of vessel and black pixels represent the background. Vessel density is defined as the percentage of the area occupied by vessels in the image, which is given by (31,32):

$$VD = \frac{\sum_{(x,y) \in area} v(x,y)}{S_{area}}, v(x,y) = \begin{cases} 1, & \text{if } (x, y) \text{ is inside a vessel} \\ 0, & \text{if } (x, y) \text{ is outside a vessel} \end{cases} \tag{1}$$

where the VD is vessel density, S_{area} is the total number of pixels in the scanning area, and the numerator indicates the number of pixels which were detected as vessels.

Statistical analysis

Statistical analyses were performed with SPSS software (V24.0, IBM Corp., Armonk, New York, USA) and JMP software (Pro 10.0.0, SAS Institute Inc., NC, USA). The results were based on the three measurements and presented as the mean±SD. The repeatability for the vessel density measurement of tissue region of interest was evaluated by the coefficient of variation (CV) and intraclass correlation coefficient (ICC). The coefficient of variation obtained for each subject was calculated and averaged among the 15 subjects. The ICC was used to measure reliability and a higher ICC commonly indicated better repeatability of the method. ICC less than 0.4 is considered as poor, between 0.4 and 0.6 as fair, between 0.6 and 0.8 as good and higher than 0.8 as excellent (33). One-way analysis of variation (ANOVA) was used to evaluate the agreement between the four positions. A P-value < 0.05 was considered as statistically significant.

3. Results

A total 15 healthy individuals participated in this study, consisting of 6 males and 9 females. All of them were Asian. The average age was 30.0±3.6 years old (range from 21 to 37 years old).

Typical vascular *en face* images of whole dermis layer, papillary layer and reticular layer are shown in Figure 2. This example comes from a 33-year-old healthy woman.

The VD, CV and ICC of papillary layer, reticular layer and whole dermis layer for the four locations are summarized in table 1. For papillary layer, reticular layer and the whole dermis layer, the mean vessel density was similar in the three sessions. The whole dermis layer of upper arm had the lowest CV of 2.0% and the reticular layer of shoulder had the highest CV of 8.1%. For all layers in the four locations CVs were better than 8.2%, demonstrating a good repeatability. In addition, the ICC values range from 0.811 to 0.940 in papillary layer, from 0.935 to 0.969 in reticular layer and from 0.854 to 0.943 in the whole dermis layer, respectively.

The mean VDs of the four locations, in all the three layers are shown in table 2. For each layer, the wrist has the highest VD, followed by upper arm, forearm and shoulder. Analysis of variation (ANOVA) showed that there was no statistically significant difference between the four locations in all the three layers.

4. Discussion

OCTA/OMAG provides an ability to non-invasively image the skin tissue beds, which has been used to visualize microvascular networks in acne (20), nail (34), scars and lesions (35). In the present study, using a faster SS-OCT system setup, we obtained high-quality images of vessel networks located within papillary layer, reticular layer and whole dermis layer, and quantified the vessel density of the three layers on wrist, forearm, shoulder and upper arm.

In the scanning period of each subject, we made effort to keep equal experimental conditions for our study, such as procedural protocol, environment temperature and experimental time. For the whole dermis of all the four locations, the CVs were no more than 2.7% and the ICC were higher than 0.854, demonstrating an excellent repeatability of VD measurement.

The VD between the four locations in all the three layers showed no statistically significant difference. This result is important for clinical translation of the OCTA/OMAG to image the skin tissue beds, to improve the diagnosis and treatment. For example, in the recovery process of large-area skin burns, the vascular density of the skin at the burn site needs to be monitored and thereafter compared to the normal area. If the skin of one site (such as the forearm) happens to be all burned, it is impossible to make comparison in the same area. At this point, the comparison between the burning wound with the normal skin of other parts (such as the upper arm) may be a practicable approach in the monitoring of recovery process.

One limitation of our study is that the size of sample is still relatively small (15 subjects). Another limitation is that we only established repeatability in healthy subjects. Patients with vascular diseases could further degrade the repeatability of the exam. Changes in morphology of vascular vessels could affect the dermal-epidermal junction, which will also potentially make it harder for the segmentation algorithms to automatically segment the physiological layers of epidermis, papillary dermis and reticular dermis, leading to reduced accuracy of vessel density measurements. Future repeatability studies should be able to resolve these concerns better.

In conclusion, our study has provided a noninvasive method to imaging vascular system using OMAG. Excellent repeatability of arm skin vessel density was obtained in healthy Asian subjects. The result also showed no significant difference of vessel density between wrist, forearm, shoulder and upper arm. These finding may help understand the variation within subjects and provide important information in distinguishing various skin abnormalities in patients.

Acknowledgments

References

1. Schmeling H, Stephens S, Goia C, Manlhiot C, Schneider R, Luthra S, Stringer E, Feldman BM. Nailfold capillary density is importantly associated over time with muscle and skin disease activity in juvenile dermatomyositis. Rheumatology. 2011; 50:885–893. [PubMed: 21156669]

2. Kharazmi, P., Lui, H., Wang, ZJ., Lee, TK. Automatic detection of basal cell carcinoma using vascular-extracted features from dermoscopy images. InElectrical and Computer Engineering (CCECE), 2016 IEEE Canadian Conference on; 2016 May 15; p. 1-4.

3. Chang CH, Tsai RK, Wu WC, Kuo SL, Yu HS. Use of dynamic capillaroscopy for studying cutaneous microcirculation in patients with diabetes mellitus. Microvasc Res. 1997; 53:121–127. [PubMed: 9143543]

4. Struijker-Boudier HAJ, Rosei AE, Bruneval P, Camici PG, Christ F, Henrion D, Lévy BI, Pries A, Vanoverschelde JL. Evaluation of the microcirculation in hypertension and cardiovascular disease. Eur Heart J. 2007; 28:2834–2840. [PubMed: 17942581]

5. Smith V, Beeckman S, Herrick AL, Decuman S, Deschepper E, De Keyser F, Distler O, Foeldvari I, Ingegnoli F, Muller-Ladner U, Riccieri V, Riemekasten G, Sulli A, Voskuyl A, Cutolo M. An EULAR study group pilot study on reliability of simple capillaroscopic definitions to describe capillary morphology in rheumatic diseases. Rheumatology (Oxford). 2016; 55:883–890. [PubMed: 26843483]

6. Micantonio T, Gulia A, Altobelli E, Di Cesare A, Fidanza R, Riitano A, Fargnoli MC, Peris K. Vascular patterns in basal cell carcinoma. J Eur Acad Dermatology Venereol. 2011; 25:358–361.

7. Serné EH, De Jongh RT, Eringa EC, IJzerman RG, Stehouwer CDA. Microvascular dysfunction: A potential pathophysiological role in the metabolic syndrome. Hypertension. 2007; 50:204–211. [PubMed: 17470716]

8. Shore AC. Capillaroscopy and the measurement of capillary pressure. Br J Clin Pharmacol. 2000; 50:501–513. [PubMed: 11136289]

9. Murray A, Gorodkin R, Moore T. Comparison of red and green laser doppler imaging of blood flow. Lasers Surg Med. 2004; 35:191–200. [PubMed: 15389741]

10. Favazza CP, Jassim O, Cornelius La, Wang LV. In vivo photoacoustic microscopy of human cutaneous microvasculature and a nevus. J Biomed Opt. 2011; 16:16015.

11. Hsu H-C, Wang L, Wang LV. In vivo photoacoustic microscopy of human cuticle microvasculature with single-cell resolution. J Biomed Opt. 2016; 21:56004. [PubMed: 27207113]

12. Zhang HF, Maslov K, Li M-L, Stoica G, Wang LV. In vivo volumetric imaging of subcutaneous microvasculature by photoacoustic microscopy. Opt Express. 2006; 14:9317–9323. [PubMed: 19529315]

13. Huang D, Swanson EA, Lin CP, Schuman JS, Stinson WG, Chang W, Hee MR, Flotte T, Gregory K, Puliafito CA, Fujimoto JG. Optical coherence tomography. Science (New York, NY). 1991; 254:1178–1181.

14. Tomlins PH, Wang RK. Theory, developments and applications of optical coherence tomography. J Phys D Appl Phy. 2005; 38:2519–2535.

15. Zhang A, Zhang Q, Chen CL, Wang RK. Methods and algorithms for optical coherence tomography-based angiography: a review and comparison. J Biomed Opt. 2015; 20:100901. [PubMed: 26473588]

16. Wang RK, An L, Francis P, Wilson DJ. Depth-resolved imaging of capillary networks in retina and choroid using ultrahigh sensitive optical microangiography. Opt Lett. 2010; 35:1467–1469. [PubMed: 20436605]

17. Chen CL, Wang RK. Optical coherence tomography based angiography [Invited]. Biomed Opt Express. 2017; 8:1056–1082. [PubMed: 28271003]

18. An L, Qin J, Wang RK. Ultrahigh sensitive optical microangiography for in vivo imaging of microcirculations within human skin tissue beds. Opt Express. 2010; 18:8220–8228. [PubMed: 20588668]

19. Qin J, Jiang J, An L, Gareau D, Wang RK. In vivo volumetric imaging of microcirculation within human skin under psoriatic conditions using optical microangiography. Lasers Surg Med. 2011; 43:122–129. [PubMed: 21384393]

20. Baran U, Li Y, Choi WJ, Kalkan G, Wang RK. High resolution imaging of acne lesion development and scarring in human facial skin using OCT-based microangiography. Lasers Surg Med. 2015; 47:231–238. [PubMed: 25740313]

21. Baran U, Shi L, Wang RK. Capillary blood flow imaging within human finger cuticle using optical microangiography. J Biophotonics. 2015; 8:46–51. [PubMed: 25590582]

22. Baran U, Qin W, Qi X, Kalkan G, Wang RK. OCT-based label-free in vivo lymphangiography within human skin and areola. Sci Rep. 2016; 6:21122. [PubMed: 26892830]

23. Baran U, Choi WJ, Wang RK. Potential use of OCT-based microangiography in clinical dermatology. Ski Res Technol. 2016; 22:238–246.

24. Choi, Woo June, Wang, RK. Volumetric cutaneous microangiography of human skin in vivo by VCSEL swept-source optical coherence tomography. Quantum Electron. 2014; 44:740–745.

25. Huang Y, Zhang Q, Thorell MR, An L, Durbin MK, Laron M, Sharma U, Gregori G, Rosenfeld PJ, Wang RK. Swept-source OCT angiography of the retinal vasculature using intensity differentiation-based optical microangiography algorithms. Ophthalmic Surg. 2014; 45:382–389.

26. Thorell MR, Zhang Q, Huang Y, An L, Durbin MK, Laron M, Sharma U, Stetson PF, Gregori G, Wang RK, Rosenfeld PJ. Swept-source OCT angiography of macular telangiectasia type 2. Ophthalmic Surg. 2014; 45:369–380.

27. Yousefi S, Zhi Z, Wang RK. Eigendecomposition-based clutter filtering technique for optical microangiography. IEEE Trans Biomed Eng. 2011; 58:2316–2323.

28. Zhang Q, Wang J, Wang RK. Highly efficient eigen decomposition based statistical optical microangiography. Quant Imaging Med Surg. 2016; 6:557–563. [PubMed: 27942476]

29. Baran U, Zhu W, Choi WJ, Omori M, Zhang W, Alkayed NJ, Wang RK. Automated segmentation and enhancement of optical coherence tomography-acquired images of rodent brain. J Neurosci Methods. 2016; 270:132–137. [PubMed: 27328369]

30. Yin X, Chao JR, Wang RK. User-guided segmentation for volumetric retinal optical coherence tomography images. J Biomed Opt. 2014; 19:086020. [PubMed: 25147962]

31. Reif R, Qin J, An L, Zhi Z, Dziennis S, Wang R. Quantifying optical microangiography images obtained from a spectral domain optical coherence tomography system. Int J Biomed Imaging. 2012; 2012:509783. [PubMed: 22792084]

32. Chu Z, Lin J, Gao C, Xin C, Zhang Q, Chen CL, Roisman L, Gregori G, Rosenfeld PJ, Wang RK. Quantitative assessment of the retinal microvasculature using optical coherence tomography angiography. J Biomed Opt. 2016; 21:066008.

33. Fleiss, JL. Reliability of Measurement. New York: John Wiley & Sons; 1986. p. 1-32.

34. Xu J, Song S, Wei W, Wang RK. Wide field and highly sensitive angiography based on optical coherence tomography with akinetic swept source. Biomed Opt Express. 2017; 8:420–435. [PubMed: 28101428]

35. Gong P, Es'haghian S, Harms KA, et al. Optical coherence tomography for longitudinal monitoring of vasculature in scars treated with laser fractionation. J Biophotonics. 2016; 9:626–636. [PubMed: 26260918]
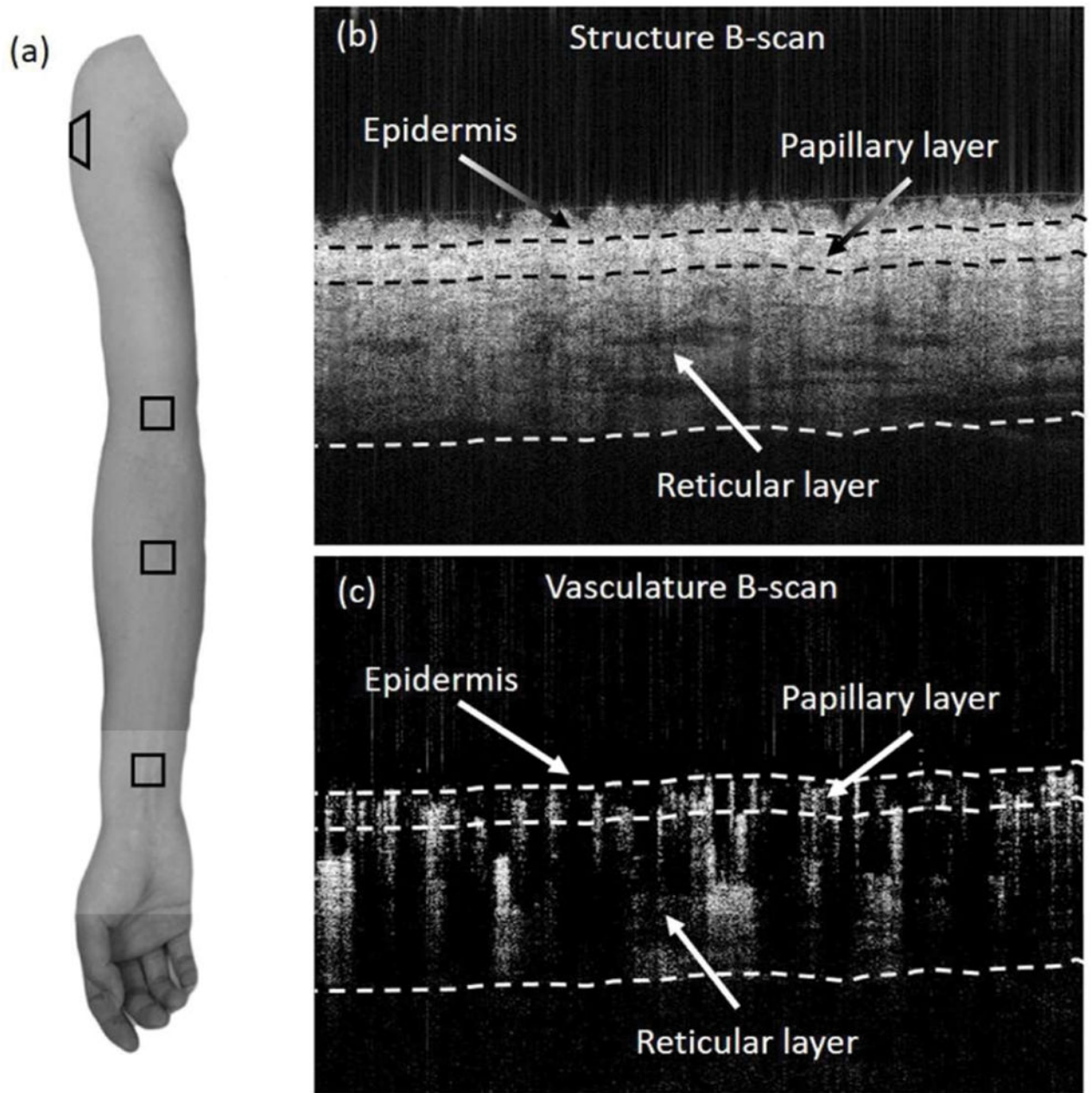
Figure 1.
(a) The arm photo of one volunteer. The box shows the imaging regions of interest at the wrist, forearm, shoulder and upper arm. (b, c) OCT cross-section images on forearm. (b) structure image; (c) OMAG image. Three layers (epidermis, papillary and reticular) are highlighted by three interfaces (dashed line).
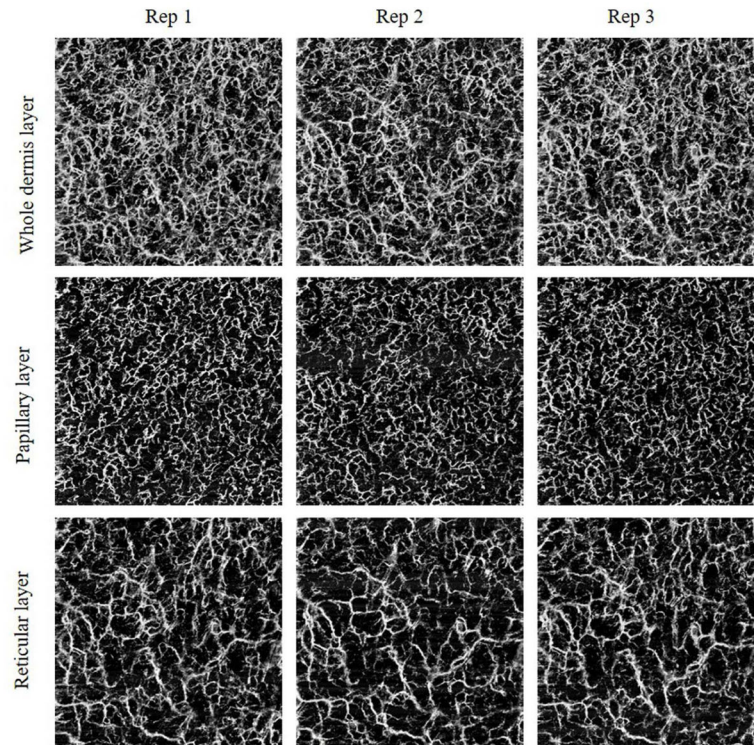
Figure 2.
Typical e*n face* images of the whole dermis layer, papillary layer, reticular layer respectively obtained from three repeated imaging sessions on one subject.

Table 1

Vessel density of three sessions and corresponding CV and ICC for each layer of the four positions.

	VD1 (%)	VD2 (%)	VD3 (%)	CV (%)	ICC (95% CI)
Wrist					
Papillary	23.2±1.7	23.4±1.8	23.3±1.6	4.4±3.3	0.896(0.658,0.957)
Reticular	23.1±4.2	23.2±4.3	22.0±3.5	5.7±4.1	0.946(0.872,0.980)
Whole dermis	40.2±2.4	40.7±3.1	40.0±2.1	2.4±1.9	0.906(0.782,0.966)
Forearm					
Papillary	21.4±4.1	21.9±3.8	21.8±3.5	6.2±5.1	0.941 (0.860,0.978)
Reticular	21.5±4.7	20.7±4.7	21.5±4.6	7.1±6.5	0.935(0.848,0.976)
Whole dermis	39.2±2.4	39.6±2.4	40.1±1.9	2.7±2.2	0.854(0.661,0.946)
Shoulder					
Papillary	21.0±2.4	21.7±2.6	21.4±2.4	5.9±4.2	0.839(0.620,0.941)
Reticular	20.6±5.0	20.4±5.4	19.1±5.1	8.1±5.0	0.959(0.901,0.985)
Whole dermis	38.3±3.4	39.3±3.2	38.4±3.2	2.7±2.0	0.943(0.846,0.976)
Upper arm					
Papillary	22.3±1.4	22.5±1.1	21.9±1.3	4.4±1.4	0.811(0.620,0.921)
Reticular	22.3±4.2	22.4±4.2	21.9±3.9	4.8±3.3	0.969(0.927,0.989)
Whole dermis	39.6±2.1	40.1±1.5	39.3±1.9	2.0±0.9	0.916(0.797,0.970)

VD: vessel density; CV: coefficient of variation; VD and CV are presented as mean±SD; ICC: intraclass correlation coefficient.

Author Manuscript

Author Manuscript

Author Manuscript

Author Manuscript

Table 2

Mean vessel density for each layer of the four positions.

	Wrist (%)	Forearm (%)	Shoulder (%)	Upper arm (%)	P-value
Papillary	23.3±1.3	21.7±3.6	21.4±2.1	22.3±0.9	0.1063
Reticular	22.8±3.8	21.3±4.4	20.0±5.0	22.2±4.0	0.3371
Whole dermis	40.3±2.4	39.6±2.0	38.7±3.1	39.7±1.8	0.3233

Vessel density is presented as mean±SD.